



Quantifying the influence of CO₂ seasonality on future aragonite undersaturation onset

T. P. Sasse¹, B. I. McNeil¹, R. J. Matear², and A. Lenton²

¹Climate Change Research Centre, Kensington Campus, University of New South Wales, Sydney, Australia

²CSIRO Oceans and Atmosphere National Research Flagship, Hobart, Australia

Correspondence to: T. P. Sasse (t.sasse@unsw.edu.au)

Received: 31 March 2015 – Published in Biogeosciences Discuss.: 22 April 2015

Revised: 18 September 2015 – Accepted: 2 October 2015 – Published: 22 October 2015

Abstract. Ocean acidification is a predictable consequence of rising atmospheric carbon dioxide (CO₂), and is highly likely to impact the entire marine ecosystem – from plankton at the base of the food chain to fish at the top. Factors which are expected to be impacted include reproductive health, organism growth and species composition and distribution. Predicting when critical threshold values will be reached is crucial for projecting the future health of marine ecosystems and for marine resources planning and management. The impacts of ocean acidification will be first felt at the seasonal scale, however our understanding how seasonal variability will influence rates of future ocean acidification remains poorly constrained due to current model and data limitations. To address this issue, we first quantified the seasonal cycle of aragonite saturation state utilizing new data-based estimates of global ocean-surface dissolved inorganic carbon and alkalinity. This seasonality was then combined with earth system model projections under different emissions scenarios (representative concentration pathways; RCPs 2.6, 4.5 and 8.5) to provide new insights into future aragonite undersaturation onset. Under a high emissions scenario (RCP 8.5), our results suggest accounting for seasonality will bring forward the initial onset of month-long undersaturation by 17 ± 10 years compared to annual-mean estimates, with differences extending up to 35 ± 16 years in the North Pacific due to strong regional seasonality. This earlier onset will result in large-scale undersaturation once atmospheric CO₂ reaches 496 ppm in the North Pacific and 511 ppm in the Southern Ocean, independent of emission scenario. This work suggests accounting for seasonality is critical to projecting the future impacts of ocean acidification on the marine environment.

1 Introduction

The global ocean currently absorbs about 30 % of annual fossil-fuel CO₂ emissions (Le Quéré et al., 2015), and will likely sequester up to 80 % of all human-derived CO₂ emissions over the coming centuries (Archer et al., 1997). While this ecosystem service largely mediates the rate of climate change, the immediate impact of this additional CO₂ is a shift in the ocean's chemical composition, resulting in lower pH and carbonate ion (CO₃²⁻) concentrations – commonly referred to as ocean acidification (OA; Caldeira and Wickett, 2003).

Of great concern to marine ecosystems is the immediate impact OA is presenting to multiple organisms. This includes organisms that require an adequate supply of CO₃²⁻ to form and preserve their calcium carbonate (CaCO₃) shells and skeletons (e.g. corals, pteropods and coccolithophorids). Two key parameters for understanding how a change in CO₃²⁻ impacts marine calcifiers are the saturation states for aragonite (Ω_{Ar} ; Eq. 1) and calcite (Ω_{Ca} ; Eq. 2) – the two main CaCO₃ minerals formed by marine calcifiers.

$$\Omega_{Ar} = [\text{Ca}^{2+}] [\text{CO}_3^{2-}] / K_{sp(Ar)}^* \quad (1)$$

$$\Omega_{Ca} = [\text{Ca}^{2+}] [\text{CO}_3^{2-}] / K_{sp(Ca)}^* \quad (2)$$

Here, [Ca²⁺] and [CO₃²⁻] represent the concentrations of calcium and carbonate ions respectively, while $K_{sp(Ar)}^*$ and $K_{sp(Ca)}^*$ are the apparent stoichiometric solubility products for aragonite and calcite. Laboratory and mesocosm experiments suggest production and dissolution of biogenic CaCO₃ are mainly controlled by seawater Ω levels (Secretariat of the Convention on Biological Diversity, 2014; Fabry et al., 2008). These experiments further indicate significant de-

creases in calcification rates when test species are exposed to Ω levels below their natural range for periods of days to weeks (Chan and Connolly, 2013). Once seawater Ω levels fall below 1, referred to as undersaturation, seawater becomes corrosive to CaCO₃ and dissolution can occur. Although experimental studies show detrimental impacts at seawater Ω levels above 1 (e.g. Bednarsek et al., 2012; Fabry et al., 2008), undersaturation is widely regarded as a key threshold value (e.g. Hunt et al., 2008; Orr et al., 2005). Since aragonite is approximately 50 % more soluble than calcite, resulting in earlier undersaturation, the focus of this work is on future changes in Ω_{Ar} .

Several previous studies have used Earth system models (ESM) to predict future annual-mean Ω_{Ar} levels under different CO₂ emission scenarios (Caldeira and Wickett, 2003, 2005; Cao et al., 2007; Kleypas et al., 1999; Orr et al., 2005; Ricke et al., 2013). These annual-mean projections suggest undersaturation will occur in the Southern Ocean and high northern latitudes within the 21st century (e.g. Orr et al., 2005). However, strong natural seasonality in oceanic CO₂ has the potential to significantly alter the onset of future undersaturation, not captured by these approaches.

McNeil and Matear (2008) first demonstrated how strong CO₂ seasonality in the Southern Ocean brings forward the initial onset of month-long aragonite undersaturation conditions by ~ 30 years relative to annual-mean projections. More recent studies in Australia's Great Barrier Reef (Shaw et al., 2013), Californian coast (Gruber et al., 2012) and Arctic Ocean (Steinacher et al., 2009) further demonstrate the importance of accounting for natural CO₂ seasonality when evaluating future OA levels.

Despite significant efforts over recent years to establish a global carbon measurement network (e.g. the Global Ocean Acidification Observation Network; www.goa-on.org; Newton et al., 2014), such a large-scale initiative remains limited by spatial and temporal variability in oceanic CO₂ coupled to the high cost of ship time, resulting in only a limited understanding of CO₂ seasonality throughout the global ocean (Monteiro et al., 2010). This represents a critical gap in our ability to understand and predict the influence of natural variability for the future onset and duration of critical OA levels.

It is important to note that ESMs do provide some insights into regional CO₂ seasonality. However, it has been shown that the current generation of ESMs do not accurately capture the observation-based magnitude and/or phase of air-sea CO₂ fluxes in most ocean regions, including the Southern Ocean, North Pacific, Indian Ocean and subpolar North Atlantic (Ishii et al., 2014; Lenton et al., 2013; Pilcher et al., 2015; Sarma et al., 2013; Schuster et al., 2009). Consequently, these models do not realistically characterize the seasonality of Ω_{Ar} .

Here, we use newly constrained data-based estimates of global ocean-surface dissolved inorganic carbon (C_T) and alkalinity (A_T) of Sasse et al. (2013b) to diagnose monthly Ω_{Ar} distributions for the nominal year of 2000. We then project

our monthly observational baselines through to 2100 using decadal trends from an ensemble of Earth system climate models (CMIP5) forced under different emissions scenarios (RCPs 2.6, 4.5 and 8.5). These results provide new insights into the influence of sea-surface seasonality on the likely onset times for future aragonite undersaturation in the global ocean.

The work presented here expands on the study of McNeil and Matear (2008) with several key improvements: (1) the global CO₂ climatologies of Sasse et al. (2013b) better reflect the latest observations and were derived using a more sophisticated method; (2) we explore the potential for CO₂ disequilibrium to evolve into the future by exploiting CMIP5 model projections; (3) we project our observational baseline using three different emission scenarios (RCP2.5, 4.5 and 8.5); (4) we apply the approach globally rather than to the Southern Ocean alone.

2 Diagnosing monthly carbon system distributions

The ocean's inorganic carbon system can be fully constrained by knowing any two parameters within its inorganic carbon constituents – partial pressure of CO₂ (pCO_2), dissolved inorganic carbon (C_T), total alkalinity (A_T) or pH (Dickson et al., 2007). Here we diagnose monthly Ω_{Ar} distributions using the $1^\circ \times 1^\circ$ C_T and A_T monthly climatologies of Sasse et al. (2013b) in combination with the World Ocean Atlas 2013 (WOA13) temperature, salinity and nutrient monthly surface distributions (objectively analysed decadal averages; Garcia et al., 2014a, b; Locarnini et al., 2013; Zweng et al., 2013). Since the C_T climatologies of Sasse et al. (2013b) were predicted for the nominal year of 2000 (see Sasse et al. (2013b) for details), the Ω_{Ar} values calculated here are also representative of this year.

All calculations were conducted using the total pH scale and carbonic acid dissociation constants of Mehrbach et al. (1973) as refitted by Dickson and Millero (1987), K_{SO_4} dissociation constant of Dickson (1990b) and boric acid dissociation constant of Dickson (1990a). Calculations of Ω_{Ar} used the K_{sp} values of Mucci (1983) and [Ca]-salinity relationship of Riley and Tongudai (1967).

To evaluate the realism of our global Ω_{Ar} predictions, we compare the network of in situ Ω_{Ar} values to our corresponding $1^\circ \times 1^\circ$ predictions for the same month and location (Fig. 1). In situ Ω_{Ar} values were calculated using measured A_T and C_T concentrations, where C_T values were first normalized to the year 2000 via observed Revelle factors and assuming constant equilibrium with the atmospheric CO₂ increase (see Sasse et al. (2013b) for details). Our data-based approach is consistent with the general pattern of high Ω_{Ar} values in the tropics which decrease poleward. Our approach also captures well the strong Ω_{Ar} gradients at $\sim 40^\circ$ north and south and local Ω_{Ar} minimas in equatorial upwelling regions (see Fig. S1 in the Supplement for monthly Ω_{Ar} dis-

tributions). Statistical analysis finds the correlation between the global in situ values and our corresponding space/month $1^\circ \times 1^\circ$ predictions to be 0.98, suggesting our approach accurately captures global open-ocean Ω_{Ar} .

We further compare our zonal mean $1^\circ \times 1^\circ$ Ω_{Ar} predictions for summer and winter to evaluate the ability of our approach to capture seasonal variability (Fig. 2). The data-based zonal pattern compares well to our general understanding of a strong winter-time minimum in the higher latitudes driven by surface cooling and strong persistent winds that ventilate deep-waters depleted in CO₃²⁻ (McNeil and Matear, 2008). The stronger winter-time minimum in the Northern Hemisphere is consistent with our findings of larger seasonal amplitudes in the North Pacific and North Atlantic compared to the Southern Ocean (see Fig. 4).

Our monthly data-based Ω_{Ar} distribution also reconfirms the contemporary ocean surface is supersaturated with respect to aragonite, showing 99.3 % of monthly ocean-surface waters with Ω_{Ar} levels greater than 1 in the year 2000. The only region where month-long undersaturation was found is in the Arctic Ocean (see Fig. S2), which is consistent with previous data-based (e.g. Mathis and Questel, 2013) and model-based (e.g. Popova et al., 2014) studies.

An independent data-based climatology for monthly ocean-surface Ω_{Ar} was presented by Takahashi et al. (2014; hereinafter referred to as T14). In their approach, global Ω_{Ar} distributions were calculated for the nominal year of 2005 on a $4^\circ \times 5^\circ$ resolution using a combination of interpolated ocean-surface $p\text{CO}_2$ and predicted A_T values via a salinity and nitrate relationship. Estimates in the equatorial Pacific were however omitted due to strong interannual variability.

Comparison between T14 and our global Ω_{Ar} values (projected to the year 2005; see Sect. 6) reveals a global correlation of 0.99, with mean Ω_{Ar} values of 2.68 and 2.72 respectively. This good agreement between two independent data-based approaches provides additional confidence in our estimated Ω_{Ar} values. Several key benefits in using our Ω_{Ar} baseline include: (1) better spatial resolution; (2) inclusion of the equatorial Pacific; (3) independent uncertainty estimates in our Ω_{Ar} predictions.

3 Quantifying uncertainties in our Ω_{Ar} predictions

The approach used here to diagnose surface Ω_{Ar} distributions includes both systematic and random sources of error. The main source of random error derives from uncertainties within the global open-ocean C_T and A_T distributions, which have been estimated to be ± 11.8 and $\pm 10.2 \mu\text{mol kg}^{-1}$ respectively (Sasse et al., 2013b). To quantify the corresponding uncertainty in our calculated Ω_{Ar} values, we applied an independent testing approach using 16,727 mixed-layer C_T and A_T independent predictions of Sasse et al. (2013b). In their approach, measurements from each cruise ($N = 470$) and time-series station ($N = 2$) were individually excluded

Table 1. Regional and global skill evaluation for predicting Ω_{Ar} (see Fig. S3 for map of spatial division).

Region	Zone ^a	RSE ^b	N^c
Arctic Ocean	1	0.22	673
Subpolar North Atlantic	2	0.13	2380
Subtropical North Atlantic	3	0.11	1205
Equatorial Atlantic	4	0.16	565
Subtropical South Atlantic	5	0.12	527
Subpolar North Pacific	6	0.18	1541
Subtropical North Pacific	7	0.15	1412
Equatorial Pacific	8	0.16	764
Subtropical South Pacific	9	0.15	1353
Subtropical north Indian	10	0.13	137
Equatorial Indian	11	0.13	481
Subtropical south Indian	12	0.11	1340
Southern Ocean	13	0.10	2923
Subantarctic waters	14	0.11	1426
Global		0.138	16 727

^a Corresponding geographical region in Fig. S3; ^b residual standard error; ^c number of measurements.

from the empirical model training phase, and then used as an independent data set to predict C_T and A_T concentrations. Here we employed this data set to calculate Ω_{Ar} values using both the in situ C_T and A_T measurements and their corresponding independent predictions. Comparison between these values revealed a global uncertainty in our Ω_{Ar} predictions to be ± 0.138 (residual standard error (RSE); Fig. 3a), with summertime and wintertime RSE values of 0.142 and 0.126 respectively (Fig. 3c, e), indicating no strong seasonal biases.

To evaluate our approach for systematic errors, we analysed the global distribution of residual errors via the independent testing approach described above (Fig. 3b). We further partitioned the residuals by season to evaluate for any temporal bias (see Fig. 3d, f). The global, summertime and wintertime residual error distributions all followed a near-normal distribution with mean residual errors of 0.004, 0.001 and 0.007 respectively. This suggests no strong global or temporal biases exist in our approach.

To assess for spatial biases, we partitioned the global independent predictions into 14 ocean regions and calculated RSE values (Table 1; see Fig. S3 for regions). Here we find all regional RSE values lie within ± 0.04 units of the global RSE (0.138), with the exception the Arctic Ocean, where the RSE value was 0.22 ($N = 673$). In particular, the Southern Ocean is where our approach excels, predicting Ω_{Ar} values to within ± 0.10 units ($N = 2923$). The small variance in regional RSE values around the global value indicates no spatial bias.

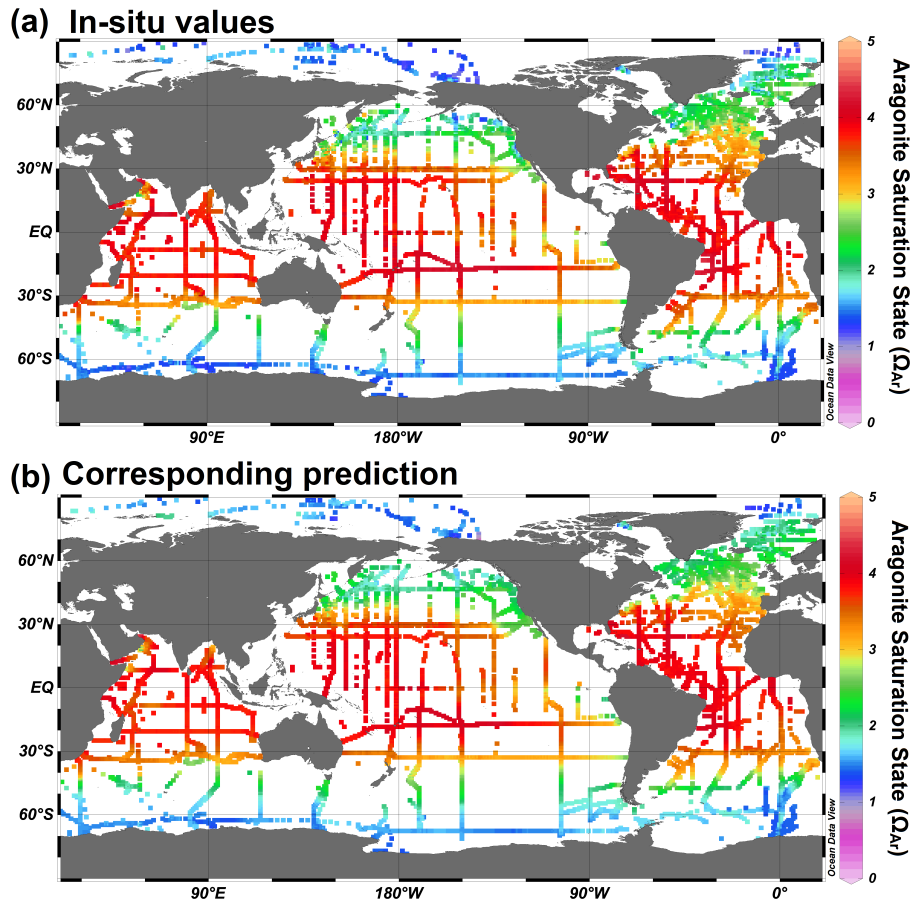


Figure 1. (a) In situ Ω_{Ar} measurements normalized to the year 2000; (b) corresponding $1^\circ \times 1^\circ$ Ω_{Ar} prediction for the same month and location for the nominal year for 2000 (see Supplement Fig. S1 for our monthly Ω_{Ar} distributions).

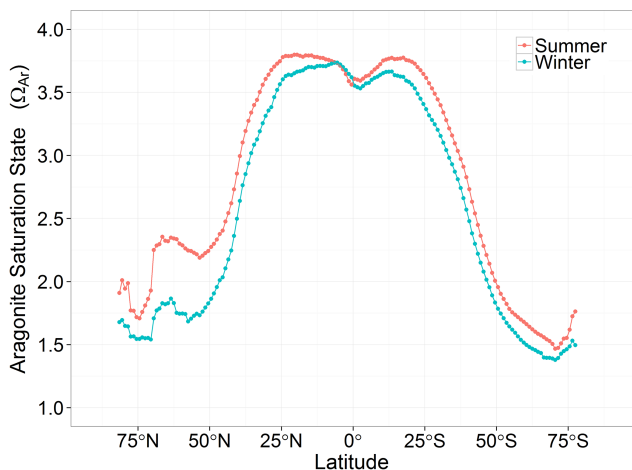


Figure 2. Zonal mean Ω_{Ar} predictions for winter and summer. Summer and winter months were defined as June through to August and December through to February for the Northern Hemisphere respectively, while Southern Hemisphere differed by 6 months.

Finally, it is important to acknowledge that uncertainties and biases in the WOA13 objectively analysed products will influence our data-derived Ω_{Ar} distributions. Since error estimates in the WAO13 products remain uncertain, this source of uncertainty cannot be accounted for at this time. However, if we assume errors in WOA13 are uncorrelated and much smaller than errors associated with the carbonate system, then they will not significantly contribute to uncertainty in our calculated Ω_{Ar} values.

4 How large is contemporary seasonal variability?

Seasonal amplitudes were calculated here as the difference between the maximum and minimum monthly Ω_{Ar} values in each $1^\circ \times 1^\circ$ grid cell (Fig. 4). From a global open-ocean perspective, seasonality was found to be 0.46 ± 0.25 (mean \pm standard deviation (1σ)), while strong regional mixing/upwelling regimes and/or biological production results in large spatial differences. In the high northern latitudes (45 to 70° N) and southern subtropics (20 to 45° S) for example, seasonality was found to be strongest at 0.73 ± 0.20

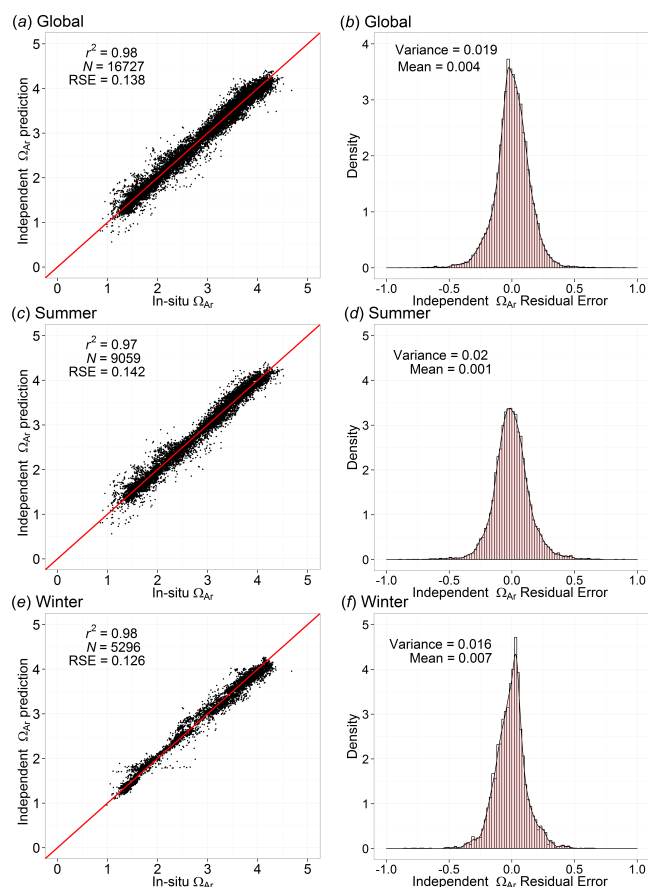


Figure 3. Statistical plots comparing global Ω_{Ar} values calculated via the network of in situ C_T and A_T measurements and independently predicted C_T and A_T values of Sasse et al. (2013b). (a) Global independent predictions versus in situ values, where the red line represents $y = x$ relationship. (b) Global distribution of independent residual errors. (c, e) Summer- and wintertime independent predictions versus in situ values. (d, f) Summer- and wintertime distribution of the independent residual errors. Summer and winter months were defined as May through to September and November through to March for the Northern Hemisphere respectively, while Southern Hemisphere differed by 6 months.

and 0.46 ± 0.14 respectively, while seasonality in the equatorial region ($20^\circ N$ to $20^\circ S$) was found to be weakest at 0.34 ± 0.21 .

From an OA perspective, regions where seasonality is strongest will have the largest implications for the future onset of critical Ω_{Ar} levels. In the tropics for example, where aragonite-secreting corals are abundant (Tupper et al., 2011), the relatively weak seasonality will result in little difference between month-long and annual-mean onset for future Ω_{Ar} levels. In the higher latitudes however, where seasonality is largest, the implications for future Ω_{Ar} onset will be much more pronounced.

It must be noted that our seasonal predictions will underestimate some coastal regions where limited data exist. Along

the coastal Antarctic continent for example, in situ data have shown seasonal Ω_{Ar} variability of up to 1.75 (McNeil et al., 2010), which is not captured by our approach.

5 Is seasonality the dominant mode of Ω_{Ar} variability?

Variability in the open-ocean CO₂ system is driven mainly by seasonal and interannual variability (IAV), with diurnal variability only playing a significant role in coastal waters (Secretariat of the Convention on Biological Diversity, 2014).

To quantify the relative roles of seasonal and IAV in open-ocean waters, we analysed results from an ensemble of six ESMs participating in the Coupled Model Intercomparison Project 5 (CMIP5; Table 2). Each model was first re-gridded to a $1^\circ \times 1^\circ$ resolution and Ω_{Ar} values calculated via the standard CO₂ dissociation constants described in Sect. 2. To constrain the total magnitude of natural variability we combined the seasonal and IAV signals within each $1^\circ \times 1^\circ$ grid cell (Fig. 5a). For IAV, we de-trended annual-mean projections from 2006 through to 2100 under the RCP8.5 emission scenario via a third-order polynomial, and then calculated the second standard deviation (2σ) in the de-trended data (i.e. 95.4 % of the year-to-year variance). For seasonality, we used the average seasonal magnitude (maximum minus minimum) between 2006 and 2016. The relative roles of variability were finally quantified by dividing the individual components by the total variability. We also multiplied these values by 100 to present the relative roles of seasonal variability and IAV as a percentage of the total natural variability (Fig. 5b, c).

This model-based analysis revealed seasonality to be the dominant mode of variability throughout the global open-ocean, accounting for $74 \pm 12\%$ (mean $\pm 1\sigma$) of total natural variability. From a regional perspective, seasonality is the dominant mode in the higher latitudes, accounting for $84 \pm 5\%$ of total variability in the Southern Ocean (south of $30^\circ S$) and North Pacific (30 to $70^\circ N$). In the eastern equatorial Pacific however, IAV is the dominant mode of variability, representing up to 70 % of total variability (Fig. 5c). With the exception of the central equatorial Pacific, seasonality is the dominant mode of variable across the greater equatorial region ($30^\circ S$ to $30^\circ N$), accounting for $67 \pm 12\%$ of the total natural variability within this region (Fig. 5b). These results are independent of the emission scenario used to calculate the seasonal and interannual variability components.

Comparison between our data-based Ω_{Ar} seasonal amplitudes (Fig. 4) and model-based total variability (Fig. 5a) reveals a similar spatial pattern in regions where seasonality is the dominant mode (i.e. North Pacific, Southern Ocean and west North Atlantic). Despite this general agreement, we find our data-based seasonal estimates are on average 1.3 times larger than the 2006–2016 model-based mean seasonal amplitudes in the North Atlantic, North Pacific and Southern Ocean ($1\sigma = 0.5$; see Fig. S4). We further compared

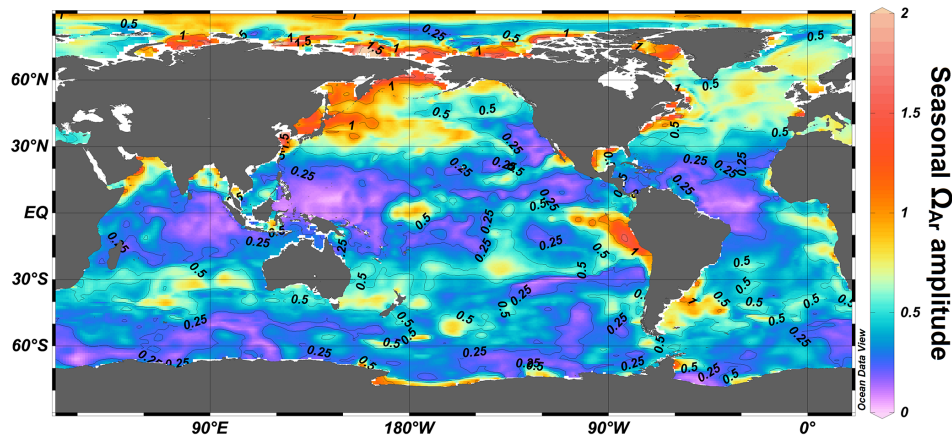


Figure 4. Seasonal Ω_{Ar} amplitudes for the nominal year of 2000. Seasonal amplitudes were calculated as the maximum minus minimum monthly Ω_{Ar} values in each $1^\circ \times 1^\circ$ cell (see Fig. S1 for monthly Ω_{Ar} distributions).

Table 2. Main characteristics of the six ESMs used in this study.

Model	Ocean resolution	Biogeochemical model	Reference
CanESM2	0.9–1.4°	CMOC	Zahariev et al. (2008)
GFDL-ESM2M	0.3–1°	TOPAZ2	Dunne et al. (2013)
HadGEM2-ES	0.3–1°	Diat-HadOCC	Palmer and Totterdell (2001)
IPSL-CM5A-LR	0.5–2°	PISCES	Aumont and Bopp (2006); Séférian et al. (2013)
IPSL-CM5A-MR	0.5–2°	PISCES	Aumont and Bopp (2006); Séférian et al. (2013)
MPI-ESM-MR	0.4°	HAMOCC5.2	Ilyina et al. (2013)

our data-based seasonal amplitudes for the year 2000 to the 2006–2016 mean seasonal amplitudes predicted by the six individual ESMs. Here we found amplification factors for our seasonal Ω_{Ar} amplitudes ranged from 0.8 to 2.3, with a mean and standard deviation of 1.3 ± 0.5 . This suggests ESMs on average under-predict the oceans' seasonal CO₂ cycle by a factor of 1.3 (or 30 %).

6 Projecting future Ω_{Ar} levels

Exchange of CO₂ between the ocean and atmosphere is driven by the air–sea gradient in $p\text{CO}_2$. Each year, approximately 70 petagrams of carbon is naturally exchanged at the air–sea interface in both directions (Sarmiento and Gruber, 2002). Comparison between ocean-surface and atmospheric $p\text{CO}_2$ reveals seasonality in the ocean is the dominant driver of this large natural CO₂ flux (Sasse et al., 2013a; Takahashi et al., 2009), which in turn is driven by biological and physical-solubility processes (Sarmiento and Gruber, 2006) – referred to here as the natural cycling of carbon.

If the natural cycling of carbon remained in a steady state throughout the last 2 centuries, the rate of increase in regionally integrated ocean-surface $p\text{CO}_2$ would have roughly tracked the atmospheric CO₂ growth rate over longer timescales (Lenton et al., 2012; Tjiputra et al., 2014). Recent

studies have however identified shifts in the oceans' natural cycling of carbon due to climate-related alterations. For example, decadal-scale trends in ocean-surface temperature (Levitus et al., 2005; Lyman et al., 2010) and salinity (Durrack and Wijffels, 2010) are influencing both the solubility of CO₂ and ocean circulation pathways, while shifting wind patterns are impacting circulation and seasonal mixing processes, resulting in either enhanced or diminished ventilation of deep waters enriched with C_T and nutrients (e.g. Le Quéré et al., 2007; Lenton et al., 2009).

Added to this climate-mediated change in oceanic CO₂ uptake, the air–sea exchange of CO₂ is a slow process (approximately 1 year equilibration time), where local physical and biological processes can cause the ocean to deviate from atmospheric CO₂. This creates a difference between the atmospheric and ocean-surface $p\text{CO}_2$ (disequilibrium). Further, as atmospheric CO₂ increases, ocean processes can cause the ocean to lag the atmospheric increase and the disequilibrium term to increase with time (McNeil and Matear, 2013). For example, in the polar regions, short residence times of surface waters and the ventilation of old CO₂-rich deep waters creates an increasing CO₂ disequilibrium, resulting in a growing difference between atmospheric and surface ocean CO₂ over time.

To account for the effects of future climate change and increasing CO₂ disequilibrium described above, we projected

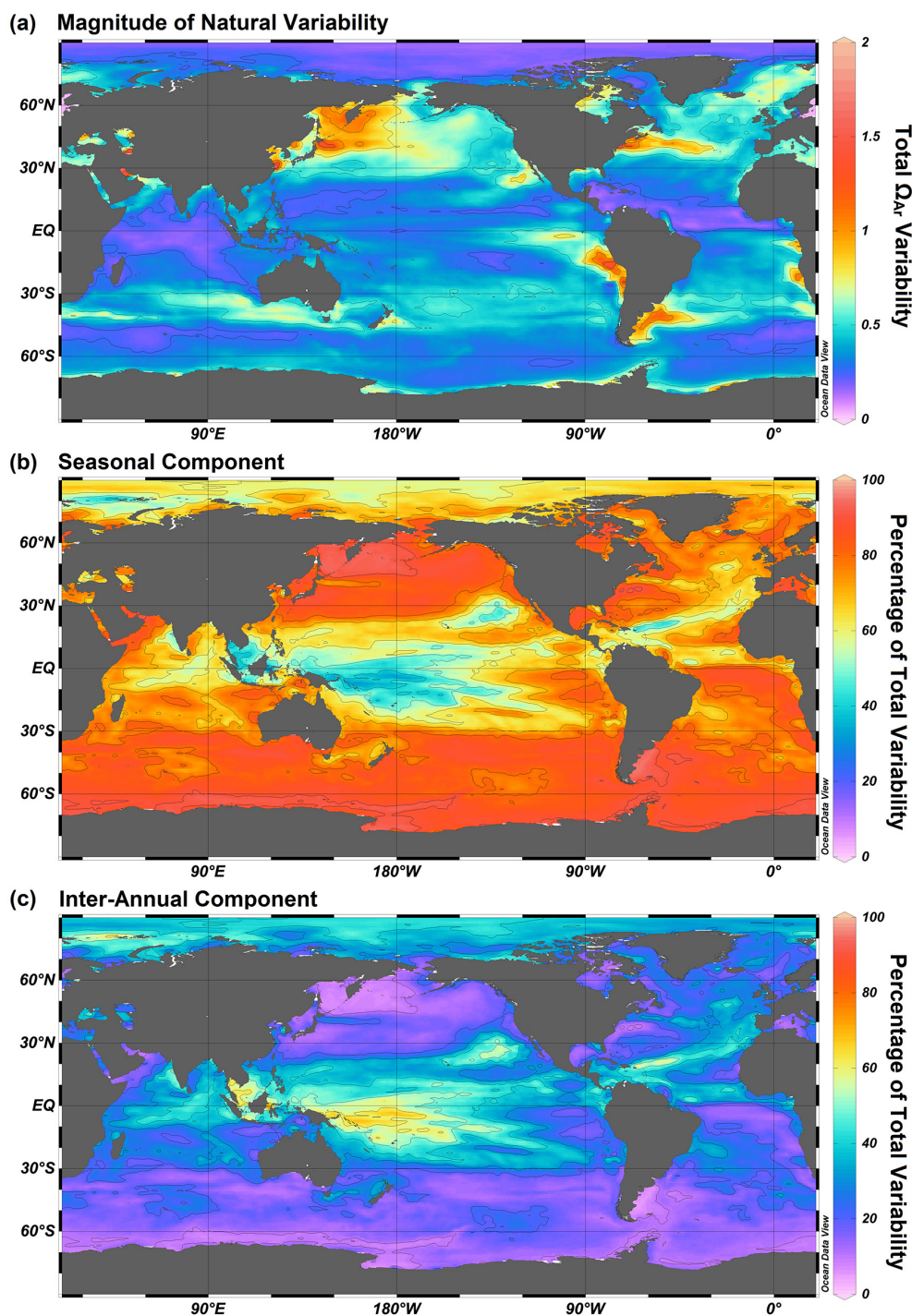


Figure 5. Model-based comparison of seasonal and interannual variability for ocean-surface Ω_{A_T} . (a) Total magnitude of variability as estimated from the ensemble of ESM. Here seasonal variability was calculated as the mean seasonal amplitude between 2006 and 2016, while IAV was calculated via the standard deviation in de-trended annual mean projections between 2006 and 2100; (b) relative contribution of seasonal variability to the total variability (in percentage); (c) relative contribution of interannual variability to the total variability (in percentage).

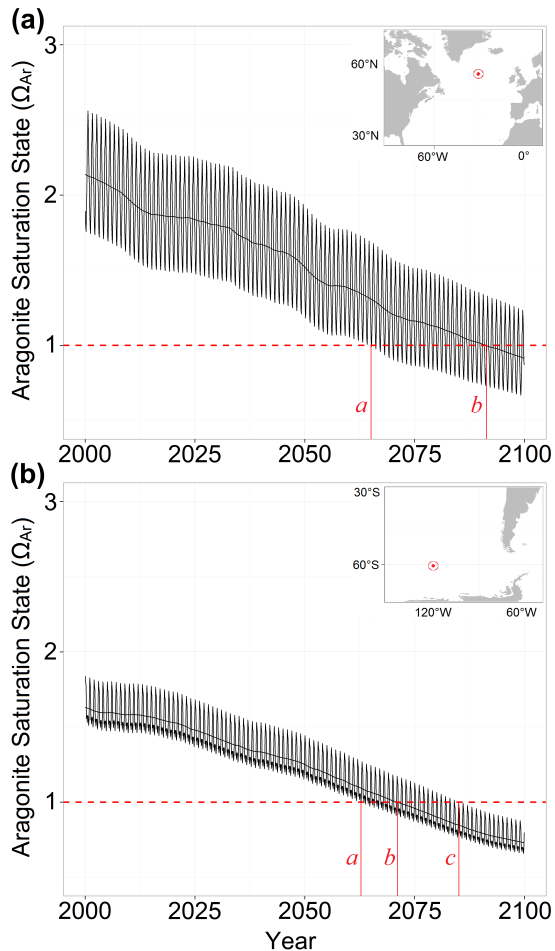


Figure 6. Future aragonite undersaturation states (Ω_{Ar}) at locations in the (a) North Atlantic and (b) Southern Ocean under the business-as-usual scenario (RCP8.5). The influence of seasonal variability accelerates undersaturation conditions by 27 and 8 years relative to annual-mean estimates (black line) in the North Atlantic and Southern Ocean respectively. The red points *a*, *b*, and *c* denote the time when month-long, annual-mean and permanent undersaturation occurs respectively.

our data-based CO₂ climatologies using results from an ensemble of six ESMs (Table 2). In this approach, decadal trends in C_T , A_T , temperature and salinity were combined with our monthly data-based C_T and A_T and WOA13 temperature and salinity products. Monthly Ω_{Ar} values were then calculated using the standard CO₂ dissociation constants presented in Sect. 2.

We projected our CO₂ baselines using ESM results forced under several different representative concentration pathways (RCP8.5, 4.5 and 2.6). Here, RCP8.5 is a business-as-usual scenario with little mitigation and peak CO₂ concentrations at 935 parts per million (ppm) in the year 2100; RCP4.5 is a scenario where emissions peak mid-century and are then slowly reduced, resulting in a peak CO₂ concentration of 538 ppm by 2100; finally, RCP2.6 is a best-case

scenario where emissions are dramatically reduced in the near future to the point where more CO₂ is absorbed by the ocean and terrestrial biosphere than emitted by human activities (Meinshausen et al., 2011).

It should be emphasized that the observation-based CO₂ climatologies of Sasse et al. (2013b) have been shown to accurately reconstruct the global pattern of present-day ocean-surface CO₂ variability. However, for this study we assume constant seasonality from our base-line CO₂ climatologies throughout the 21st century. Although this assumption is likely adequate for short temporal projections (< 10 years), a recent evaluation of 10 ESMs suggests large changes in mixing, biological production and CO₂ solubility will occur within the 21st century (Bopp et al., 2013). By projecting our base-line climatologies using decadal trends from ESM, we implicitly capture the decadal response to these changes; however, any potential shift in the phase and magnitude of CO₂ seasonality are not explored in our approach.

Given the limitations in the current generation of ESM in capturing seasonality in air–sea CO₂ flux and/or ocean-surface $p\text{CO}_2$ in many important regions (Ishii et al., 2014; Lenton et al., 2013; Pilcher et al., 2015; Sarma et al., 2013; Schuster et al., 2009), their ability to realistically project future changes in CO₂ seasonality is questionable. We therefore do not account for any change in CO₂ seasonality in the current study. Once models evolve to a point where seasonality of the carbon system is well-represented, potential future changes to seasonality will need to be explored in future studies.

As a first step to assessing the sensitivity of future Ω_{Ar} predictions to shifts in oceanic CO₂ seasonality, we applied the following approach to model output from six ESMs (Table 2). Seasonal cycles in C_T , A_T , temperature and salinity were first averaged over the decades 2006 through to 2015 and 2091 through to 2100 in each $1^\circ \times 1^\circ$ grid cell. Decadal-mean values from the 2091–2100 period were then added to the 2006–2015 mean seasonal cycles, thereby shifting the earlier seasonal cycle to typical values of the years 2090–2100. Finally, seasonal Ω_{Ar} values were computed using both the mean 2091–2100 and shifted 2006–2015 seasonal C_T , A_T , temperature and salinity values. Comparing the seasonal amplitudes in Ω_{Ar} found shifted values were on average 5.4% larger than the 2091–2100 period for the global open-ocean ($1\sigma = 48\%$), with individual model differences ranging from -0.4 to 19.1% . This suggests our data-based Ω_{Ar} amplitudes are on average 5.4% larger than expected if changes in C_T , A_T , temperature and salinity seasonality were taken into account.

7 Quantifying the onset of aragonite undersaturation

When strong natural carbon seasonality is combined with a long-term trend, the onset and exposure times of biological thresholds are influenced. To illustrate this point, we

present Ω_{Ar} projections under the business-as-usual scenario (RCP8.5) at two $1^\circ \times 1^\circ$ sites in the North Atlantic and Southern Ocean which are somewhat representative of the larger region (Fig. 6). At the North Atlantic site, strong seasonality was found to bring forward the initial onset (time *a* in Fig. 6a) of aragonite undersaturation by 27 years relative to the annual-mean (time *b*; Fig. 6a), while weaker variability at the Southern Ocean site brings forward undersaturation by 8 years (Fig. 6b). It is important to emphasize that monthly undersaturation conditions starts at time *a*, and then eventually extends to be permanent over all months (time *c*). As much as seasonality brings forward the initial onset of undersaturation, it also delays the permanent onset (Fig. 6). At the Southern Ocean site for example, seasonality delays the permanent onset by ~ 15 years compared to the annual mean. In the context of ocean acidification impacts, monthly exposure times are important, since laboratory experiments show that even short exposure times (i.e. hours to days) can result in significant implications to the health and well-being of the test species (Chan and Connolly, 2013).

7.1 Future Ω_{Ar} levels under RCP8.5

Under the business-as-usual scenario (RCP8.5), our results show annual-mean aragonite undersaturation will occur by the year 2086 ± 9 (mean $\pm 1\sigma$) in the North Pacific and North Atlantic, 2074 ± 12 in the Southern Ocean, while tropical and temperate regions ($\sim 40^\circ$ S to $\sim 40^\circ$ N) will remain super-saturated beyond the year 2100 (Fig. 7a). When seasonality is considered, the initial month-long onset precedes annual-mean estimates by a global average of 17 ± 10 years under the RCP8.5 scenario (70° N to 70° S; Fig. 7b–c). In the North Pacific and North Atlantic, where seasonality is strongest, month-long undersaturation is brought forward by 36 ± 16 and 19 ± 6 years respectively (Fig. 7c).

In the Southern Ocean (south of 60° S), our results show month-long aragonite undersaturation will first occur as early as the year 2030, or when atmospheric CO₂ concentrations reach ~ 450 ppm. While this is consistent with projections by McNeil and Matear (2008) under the IPCC IS92a scenario, our results show seasonality will delay the onset of annual-mean undersaturation by 14 ± 7 years, which is half the delay time found by McNeil and Matear (2008). This difference likely reflects the faster rate of change in atmospheric CO₂ under RCP8.5 compared to IPCC IS92a, while differences in seasonality found by the two approaches is likely a secondary factor.

Widespread onset of permanent Ω_{Ar} undersaturation is only found in the Southern Ocean and Arctic Ocean by the year 2100 (see Fig. S5). In the Southern Ocean, the average time difference between annual-mean and permanent onset is 13.0 ± 5.3 years, which is similar to the time difference found between annual-mean and month-long onset at the same locations (13.0 ± 5.9 years). Despite these similar basin-wide time difference values, the correlation coefficient

was found to be 0.31, indicating significant spatial differences. This reflects the non-symmetrical nature of seasonal Ω_{Ar} cycles in some regions of the Southern Ocean, as observed in Fig. 6b, which further highlights the importance of accounting for seasonal processes.

Early aragonite undersaturation is of particular concern for the many important calcifying organisms that inhabit the higher latitudes. Pteropods for example, are a zooplankton species that form aragonite shells to provide ballast for vertical migration in search of food and breeding. In the Southern Ocean, pteropods have been found to represent up to 30 % of total zooplankton (Hunt et al., 2008), and are themselves important prey for larger zooplankton, as well as many fish and bird species (Hunt et al., 2008; Karnovsky et al., 2008). From a biogeochemical perspective, pteropods account for at least 12 % of the global CaCO₃ flux into the ocean interior (Berner and Honjo, 1981). When pteropods sink to depths at which $\Omega_{Ar} = 1$, known as the saturation horizon or lysocline, field studies show significant dissolution occurs (Hunt et al., 2008). As more anthropogenic CO₂ enters the ocean system, the aragonite saturation horizon will approach the upper ocean until the surface waters become permanently undersaturated. Decade(s) before this occurs however, seasonality will expose calcifying organisms to month-long undersaturation conditions, causing unknown changes to the health and well-being of the wider marine ecosystem.

7.2 Future Ω_{Ar} levels under RCP 4.5 and 2.6

In the previous section we presented results under the RCP8.5 scenario. We now explore how lower emission scenarios influence the future onset of aragonite undersaturation. We consider our Ω_{Ar} projections under RCP4.5, 2.6 and their behaviour relative to RCP8.5 (Table 3 and Fig. 8). In the North Pacific, we find month-long aragonite undersaturation occurs by the year 2057 ± 24 and 2040 ± 15 under RCP4.5 and 8.5 respectively. Despite this difference in onset year, atmospheric CO₂ concentrations at time of onset are consistent at 492 ± 45 ppm and 501 ± 60 for RCP4.5 and 8.5 respectively, with a correlation coefficient of 0.75 (Table 3). As expected, this suggests undersaturation onset is highly dependent on the atmospheric CO₂ concentration, where we find large-scale undersaturation in the North Pacific once atmospheric CO₂ reaches 496 ppm (mean of RCP4.5 and 8.5). Similarly, our results suggest widespread aragonite undersaturation will occur when atmospheric CO₂ reaches concentrations of 517 ppm in the North Atlantic and 511 ppm in the Southern Ocean.

Under RCP2.6, whereby emissions are drastically reduced in the near future, our results show very sparse undersaturation onset in the major ocean basins by the year 2100 (Fig. 8). When compared to projections under RCP8.5, we find a 92.6 % (or 83.6×10^6 km²) reduction in global open-ocean surface waters exposed to at least month-long aragonite undersaturation within the 21st century. Regionally,

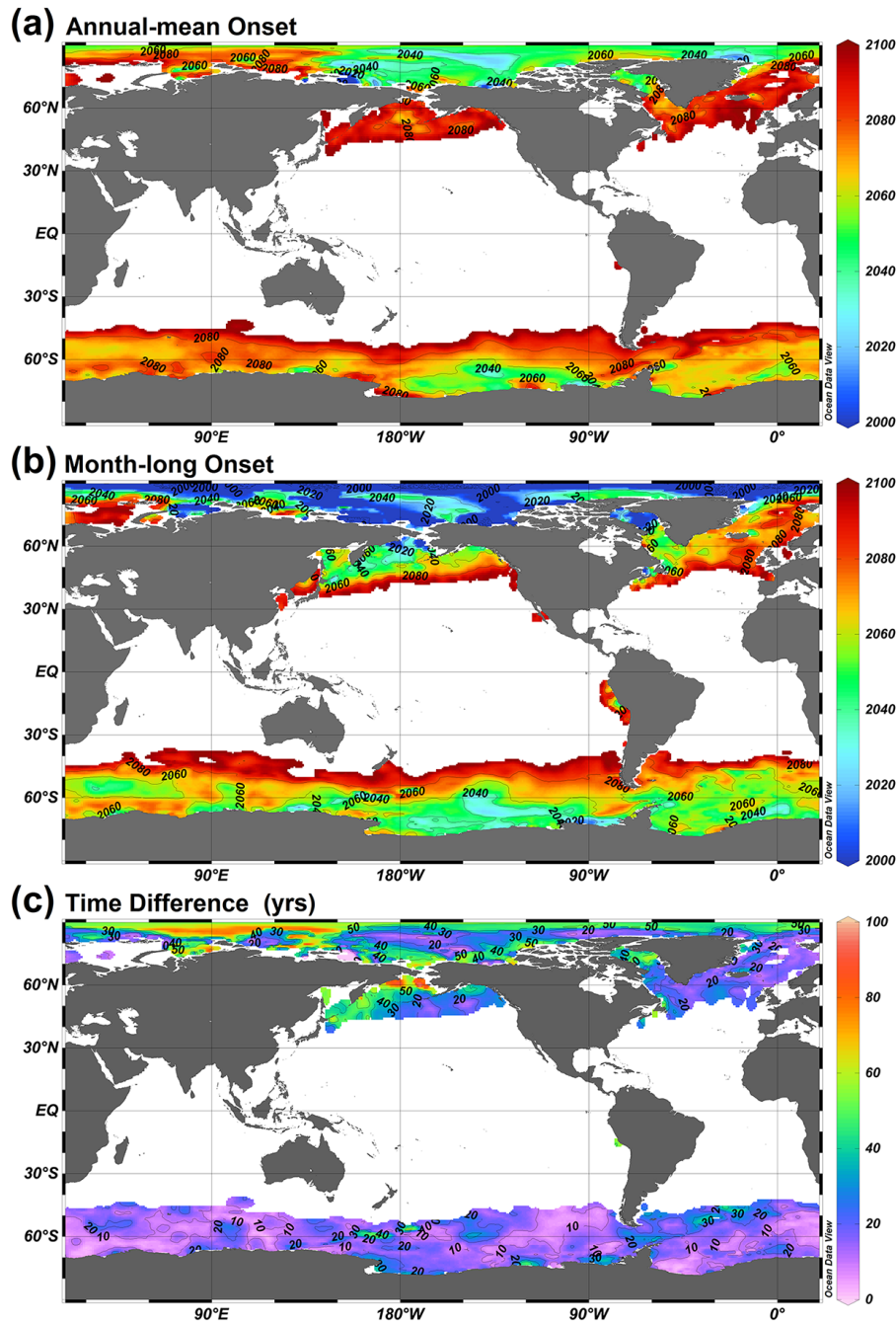


Figure 7. Estimated onset year for aragonite undersaturation under RCP8.5 for (a) annual-mean and (b) 1-month onset. (c) Time difference (years) between annual-mean and month-long estimates.

this reduction increases to 98.9 % ($62.8 \times 10^6 \text{ km}^2$), 92.8 % ($9.16 \times 10^6 \text{ km}^2$) and 99.2 % ($6.8 \times 10^6 \text{ km}^2$) in the Southern Ocean, North Pacific and North Atlantic respectively. This result highlights the potential difference humanity can make by reducing CO₂ emissions in the near future.

To further probe the influence of a lower emission scenario on future OA onset, we compare the time difference between month-long and annual-mean aragonite undersaturation on-

set under RCP8.5 and RCP4.5 at $457 1^\circ \times 1^\circ$ grid cell locations in the Southern Ocean (Figs. 8a and 7b). Here we find the average onset for month-long undersaturation occurs by the year 2048 under RCP8.5, and by 2073 under RCP4.5. Despite the lower emission scenario delaying the initial onset, we find that the time difference between month-long and annual mean onset is 18 years longer under RCP4.5 compared to RCP8.5 (i.e. 14 years under RCP8.5 and 32 years under

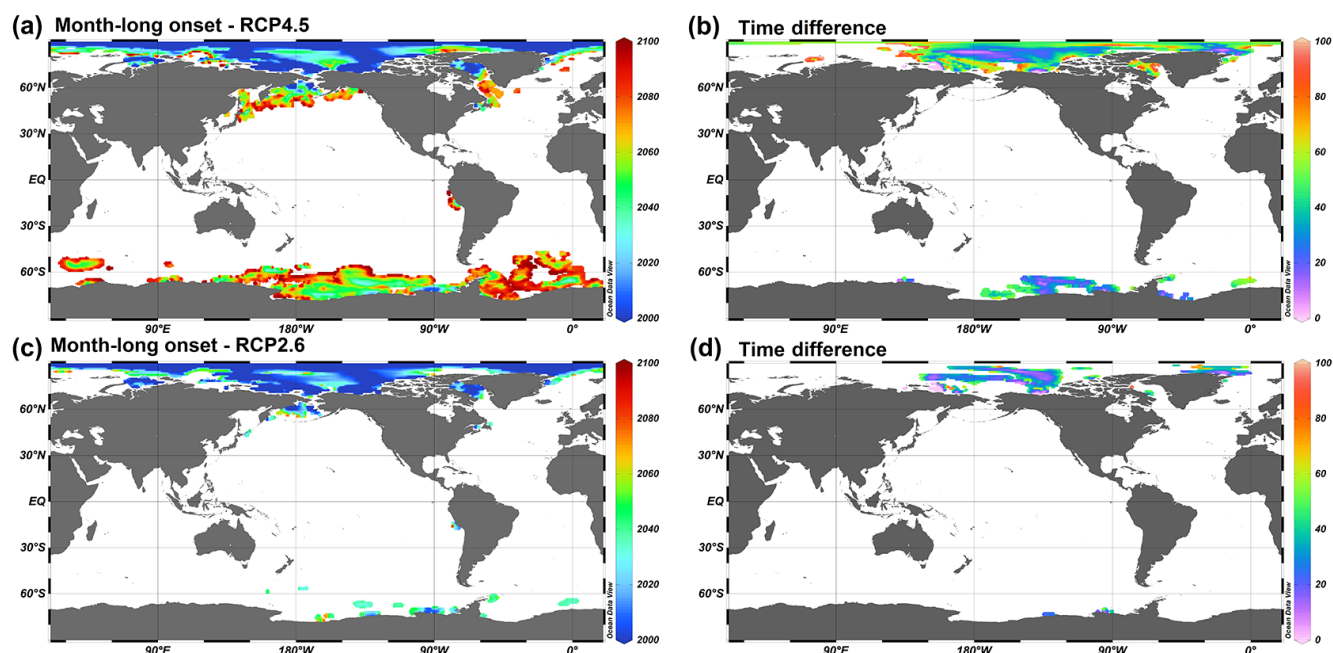


Figure 8. Onset year for month-long ocean-surface aragonite undersaturation for (a) RCP4.5 and (c) RCP2.6. Time difference (years) between month-long and annual-mean surface aragonite undersaturation onset under (b) RCP4.5 and (d) RCP2.6.

Table 3. Comparison between future aragonite projections under RCP4.5 and 2.6 relative to RCP8.5.

RCP	Month-long onset mean $\pm 1\sigma$ (RCP8.5)	Atmospheric CO ₂ mean $\pm 1\sigma$ (RCP8.5)	Corr. to RCP8.5	Number of $1^\circ \times 1^\circ$ grid cells
North Pacific (30 to 65° N)				
4.5	2057 \pm 24 (2040 \pm 15)	492 \pm 45 (501 \pm 61)	0.75	475
2.6	2022 \pm 21 (2022 \pm 15)	406 \pm 28 (428 \pm 46)	0.81	110
North Atlantic (30 to 70° N)				
4.5	2061 \pm 17 (2047 \pm 12)	505 \pm 36 (530 \pm 51)	0.86	37
2.6	2024 \pm 20 (2016 \pm 15)	415 \pm 39 (410 \pm 40)	0.88	3
Southern Ocean (south of 45° S)				
4.5	2064 \pm 19 (2045 \pm 9)	505 \pm 30 (518 \pm 46)	0.75	2619
2.6	2033 \pm 15 (2030 \pm 8)	428 \pm 19 (450 \pm 29)	0.66	154

RCP4.5). This longer time delay under RCP4.5 emphasizes that seasonality becomes even more important when projecting future OA levels under a slower emissions scenario.

8 How does seasonality influence the geographical extent of aragonite undersaturation?

Accounting for seasonality also presents significant implications for the spatial pattern of future aragonite undersaturation. Here we refer to regions where seasonality induces at least month-long undersaturation conditions, while annual-mean Ω_{Ar} projections remain super-saturated throughout the

21st century. By the year 2100, the latitudinal extent of ocean surface exposed to at least month-long aragonite undersaturation will have shifted equatorward by $\sim 3.5^\circ$ relative to the extent of annual-mean estimates under the RCP8.5 scenario (Fig. 9). This extension translates to $\sim 23 \times 10^6$ km² of open-ocean surface (or 6.8 % of total open-ocean area) exposed to at least month-long aragonite undersaturation by 2100 under the business-as-usual scenario (RCP8.5). This expansion of corrosive aragonite conditions is likely to impact multiple marine calcifiers living within these regions much earlier than anticipated under previous annual-mean projections (e.g. Orr et al., 2005). Pteropods for example, represent up to

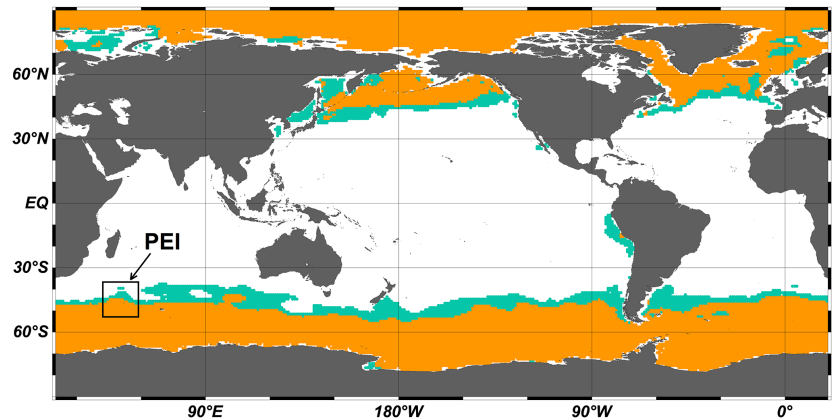


Figure 9. Surface area exposed to at least month-long (blue) and annual-mean (orange) aragonite undersaturation in the year 2100 under RCP8.5. The blue region represents $\sim 23 \times 10^6$ km². The area labelled PEI represents the pteropod study region of Hunt et al. (2008) around the Prince Edward Islands.

30 % of total zooplankton species around the Prince Edward Islands (PEI; Fig. 9; Hunt et al., 2008); if these stocks deplete under future OA levels, the many other animals that rely on pteropods as a source of food will also be detrimentally impacted.

9 Conclusion

Ocean acidification is a global issue which is likely to impact the entire marine ecosystem – from plankton at the base of the food chain to fish at the top. Of particular concern is the decreasing concentration of CO₃²⁻ ions, which lowers the saturation states of CaCO₃ minerals (Ω_{Ar} and Ω_{Ca}) and results in detrimental seawater conditions for marine calcifiers (e.g. pteropods and corals; Aze et al., 2014; Fabry et al., 2008). Predicting when critical Ω_{Ar} threshold values will be reached is crucial for projecting the future health of marine ecosystems and for marine resources planning and management. Here we have assessed how seasonality in oceanic CO₂ will influence the future onset of Ω_{Ar} undersaturation.

The influence of seasonality was evaluated by comparing the difference in future month-long and annual-mean Ω_{Ar} undersaturation onset. Our results suggest seasonality brings forward the initial onset of month-long undersaturation by 17 ± 10 years compared to annual mean estimates under RCP8.5, with differences extending up to 35 ± 17 years in the North Pacific due to strong regional seasonality.

Our results also show large-scale undersaturation once atmospheric CO₂ reaches 496 ppm in the North Pacific, 517 ppm in the North Atlantic and 511 ppm in the Southern Ocean, independent of emission scenario. It is important to note that seasonality in these regions was also found to be the dominate mode of variability, accounting for 84 ± 5 % of total model-based variability in the Southern Ocean (south of 30° S) and North Pacific (30 to 70° N). This suggests IAV will not significantly alter onset times found in this study.

Under lower emission scenarios, the average time difference between month-long and annual-mean aragonite undersaturation onset increased from 14 years under RCP8.5 to 32 years under RCP4.5 in the Southern Ocean. This larger time difference under a lower emissions scenario emphasizes the importance of accounting for seasonality when projecting future OA levels under a slower emissions scenario. The spatial extent of Ω_{Ar} undersaturation is also drastically reduced under a lower emission scenario. Under RCP2.6 for example, our results show a 92.6 % (or 83.6×10^6 km²) reduction in open-ocean exposure to Ω_{Ar} undersaturation compared to projections under RCP8.5, emphasizing the importance of mitigating CO₂ emissions.

Seasonality also presents significant implications for the spatial pattern of future Ω_{Ar} undersaturation. Here we found month-long undersaturation extended equatorward by a global average of 3.5° (or 23×10^6 km²) compared to annual-mean projections under RCP8.5. From a biogeochemical perspective, this is particularly concerning given the regions of expansion from the poles (~ 40 to 50° south and north) are known as important hotspots for CaCO₃ export (Sarmiento and Gruber, 2006).

Finally, the implication of our results is not limited to the higher latitudes; strong Ω_{Ar} seasonality in some subtropical regions (30° S to 30° N; see Fig. 4) will likely bring forward the onset of lower Ω_{Ar} waters by similar temporal periods. Since these regions are rich with sensitive calcifying coral reef ecosystems, considering the influence of seasonality is important when estimating future OA levels and their impacts in these regions.

The Supplement related to this article is available online at doi:10.5194/bg-12-6017-2015-supplement.

Acknowledgements. T. P. Sasse would like to acknowledge the funding support from the CSIRO carbon cluster, and the developers of the ocean data view program (Schlitzer et al., 2013). A. Lenton and R. J. Matear would like to acknowledge the funding support of CSIRO Oceans and Atmosphere and the Australian Climate Change Science Program.

Edited by: J. Middelburg

References

- Archer, D., Kheshgi, H., Maier, and Reimer, E.: Multiple timescales for neutralization of fossil fuel CO₂, *Geophys. Res. Lett.*, 24, 405–408, doi:10.1029/97gl00168, 1997.
- Aumont, O. and Bopp, L.: Globalizing results from ocean in situ iron fertilization studies, *Global Biogeochem. Cy.*, 20, GB2017, doi:10.1029/2005gb002591, 2006.
- Bednarek, N., Tarling, G. A., Bakker, D. C. E., Fielding, S., Jones, E. M., Venables, H. J., Ward, P., Kuzirian, A., Leze, B., Feely, R. A., and Murphy, E. J.: Extensive dissolution of live pteropods in the Southern Ocean, *Nat. Geosci.*, 5, 881–885, doi:10.1038/ngeo1635, 2012.
- Berner, R. A. and Honjo, S.: Pelagic Sedimentation of Aragonite: Its Geochemical Significance, *Science*, 211, 940–942, doi:10.1126/science.211.4485.940, 1981.
- Bopp, L., Resplandy, L., Orr, J. C., Doney, S. C., Dunne, J. P., Gehlen, M., Halloran, P., Heinze, C., Ilyina, T., Séférian, R., Tjiputra, J., and Vichi, M.: Multiple stressors of ocean ecosystems in the 21st century: projections with CMIP5 models, *Biogeosciences*, 10, 6225–6245, doi:10.5194/bg-10-6225-2013, 2013.
- Caldeira, K. and Wickett, M. E.: Oceanography: Anthropogenic carbon and ocean pH, *Nature*, 425, 365–365, doi:10.1038/425365a, 2003.
- Caldeira, K. and Wickett, M. E.: Ocean model predictions of chemistry changes from carbon dioxide emissions to the atmosphere and ocean, *J. Geophys. Res.-Oceans*, 110, C09S04, doi:10.1029/2004JC002671, 2005.
- Cao, L., Caldeira, K., and Jain, A. K.: Effects of carbon dioxide and climate change on ocean acidification and carbonate mineral saturation, *Geophys. Res. Lett.*, 34, L05607, doi:10.1029/2006gl028605, 2007.
- Chan, N. C. S. and Connolly, S. R.: Sensitivity of coral calcification to ocean acidification: a meta-analysis, *Glob. Change Biol.*, 19, 282–290, doi:10.1111/gcb.12011, 2013.
- Dickson, A. G.: Thermodynamics of the dissociation of boric acid in synthetic seawater from 273.15 to 318.15 K, *Deep-Sea Res.*, 37, 755–766, doi:10.1016/0198-0149(90)90004-F, 1990a.
- Dickson, A. G.: Standard potential of the reaction: $\text{AgCl}(s) + 1/2\text{H}_2(g) = \text{Ag}(s) + \text{HCl}(aq)$, and the standard acidity constant of the ion HSO_4^- in synthetic sea water from 273.15 to 318.15 K, *J. Chem. Thermodyn.*, 22, 113–127, doi:10.1016/0021-9614(90)90074-Z, 1990b.
- Dickson, A. G. and Millero, F. J.: A comparison of the equilibrium constants for the dissociation of carbonic acid in seawater media, *Deep-Sea Res.*, 34, 1733–1743, doi:10.1016/0198-0149(87)90021-5, 1987.
- Dickson, A. G., Sabine, C. L., and Christian, J. R. (Eds.): Guide to best practices for ocean CO₂ measurements, PICES Special Publication 3, 191 pp., 2007.
- Dunne, J. P., John, J. G., Shevliakova, E., Stouffer, R. J., Krasting, J. P., Malyshev, S. L., Milly, P. C. D., Sentman, L. T., Adcroft, A. J., Cooke, W., Dunne, K. A., Griffies, S. M., Hallberg, R. W., Harrison, M. J., Levy, H., Wittenberg, A. T., Phillips, P. J., and Zadeh, N.: GFDL's ESM2 Global Coupled Climate–Carbon Earth System Models. Part II: Carbon System Formulation and Baseline Simulation Characteristics, *J. Climate*, 26, 2247–2267, doi:10.1175/JCLI-D-12-00150.1, 2013.
- Durack, P. J. and Wijffels, S. E.: Fifty-Year Trends in Global Ocean Salinities and Their Relationship to Broad-Scale Warming, *J. Climate*, 23, 4342–4362, doi:10.1175/2010jcli3377.1, 2010.
- Fabry, V. J., Seibel, B. A., Feely, R. A., and Orr, J. C.: Impacts of ocean acidification on marine fauna and ecosystem processes, *ICES J. M. Sci.*, 65, 414–432, doi:10.1093/icesjms/fsn048, 2008.
- Garcia, H. E., Locarnini, R. A., Boyer, T. P., Antonov, J. I., Baranova, O. K., Zweng, M. M., Reagan, J. R., and Johnson, D. R.: World Ocean Atlas 2013, Volume 3: Dissolved Oxygen, Apparent Oxygen Utilization, and Oxygen Saturation, in, edited by: Levitus, S. and Mishonov, A., NOAA Atlas NESDIS 75, 27 pp., 2014a.
- Garcia, H. E., Locarnini, R. A., Boyer, T. P., Antonov, J. I., Baranova, O. K., Zweng, M. M., Reagan, J. R., and Johnson, D. R.: World Ocean Atlas 2013, Volume 4: Dissolved Inorganic Nutrients (phosphate, nitrate, silicate), edited by: Levitus, S., and Mishonov, A., NOAA Atlas NESDIS 76, 25, 25 pp. 2014b.
- Gruber, N., Hauri, C., Lachkar, Z., Loher, D., Frölicher, T. L., and Plattner, G.-K.: Rapid Progression of Ocean Acidification in the California Current System, *Science*, 337, 220–223, doi:10.1126/science.1216773, 2012.
- Hunt, B. P. V., Pakhomov, E. A., Hosie, G. W., Siegel, V., Ward, P., and Bernard, K.: Pteropods in Southern Ocean ecosystems, *Prog. Oceanogr.*, 78, 193–221, doi:10.1016/j.pocean.2008.06.001, 2008.
- Ilyina, T., Six, K. D., Segschneider, J., Maier-Reimer, E., Li, H., and Núñez-Riboni, I.: Global ocean biogeochemistry model HAMOCC: Model architecture and performance as component of the MPI-Earth system model in different CMIP5 experimental realizations, *Journal of Advances in Modeling Earth Systems*, 5, 287–315, doi:10.1029/2012MS000178, 2013.
- Ishii, M., Feely, R. A., Rodgers, K. B., Park, G.-H., Wanninkhof, R., Sasano, D., Sugimoto, H., Cosca, C. E., Nakaoka, S., Telszewski, M., Nojiri, Y., Mikaloff Fletcher, S. E., Niwa, Y., Patra, P. K., Valsala, V., Nakano, H., Lima, I., Doney, S. C., Buitenhuis, E. T., Aumont, O., Dunne, J. P., Lenton, A., and Takahashi, T.: Air–sea CO₂ flux in the Pacific Ocean for the period 1990–2009, *Biogeosciences*, 11, 709–734, doi:10.5194/bg-11-709-2014, 2014.
- Karnovsky, N. J., Hobson, K. A., Iverson, S., and Hunt, G. L. J.: Seasonal changes in diets of seabirds in the North Water Polynya: a multiple-indicator approach, *Mar. Ecol. Prog.-Ser.*, 357, 291–299, doi:10.3354/meps07295, 2008.
- Kleypas, J. A., Buddemeier, R. W., Archer, D., Gattuso, J.-P., Langdon, C., and Opdyke, B. N.: Geochemical consequences of increased atmospheric carbon dioxide on coral reefs, *Science*, 284, 118–120, doi:10.1126/science.284.5411.118, 1999.
- Lenton, A., Codron, F., Bopp, L., Metzl, N., Cadule, P., Tagliabue, A., and Le Sommer, J.: Stratospheric ozone depletion reduces

- ocean carbon uptake and enhances ocean acidification, *Geophys. Res. Lett.*, 36, L12606, doi:10.1029/2009gl038227, 2009.
- Lenton, A., Metzl, N., Takahashi, T., Kuchinke, M., Matear, R. J., Roy, T., Sutherland, S. C., Sweeney, C., and Tilbrook, B.: The observed evolution of oceanic pCO₂ and its drivers over the last two decades, *Global Biogeochem. Cy.*, 26, GB2021, doi:10.1029/2011gb004095, 2012.
- Lenton, A., Tilbrook, B., Law, R. M., Bakker, D., Doney, S. C., Gruber, N., Ishii, M., Hoppema, M., Lovenduski, N. S., Matear, R. J., McNeil, B. I., Metzl, N., Mikaloff Fletcher, S. E., Monteiro, P. M. S., Rödenbeck, C., Sweeney, C., and Takahashi, T.: Sea-air CO₂ fluxes in the Southern Ocean for the period 1990–2009, *Biogeosciences*, 10, 4037–4054, doi:10.5194/bg-10-4037-2013, 2013.
- Le Quéré, C., Rödenbeck, C., Buitenhuis, E. T., Conway, T. J., Langenfelds, R., Gomez, A., Labuschagne, C., Ramonet, M., Nakazawa, T., Metzl, N., Gillett, N., and Heimann, M.: Saturation of the Southern Ocean CO₂ Sink Due to Recent Climate Change, *Science*, 316, 1735–1738, doi:10.1126/science.1136188, 2007.
- Le Quéré, C., Moriarty, R., Andrew, R. M., Peters, G. P., Ciais, P., Friedlingstein, P., Jones, S. D., Sitch, S., Tans, P., Arneeth, A., Boden, T. A., Bopp, L., Bozec, Y., Canadell, J. G., Chini, L. P., Chevallier, F., Cosca, C. E., Harris, I., Hoppema, M., Houghton, R. A., House, J. I., Jain, A. K., Johannessen, T., Kato, E., Keeling, R. F., Kitidis, V., Klein Goldewijk, K., Koven, C., Landa, C. S., Landschützer, P., Lenton, A., Lima, I. D., Marland, G., Mathis, J. T., Metzl, N., Nojiri, Y., Olsen, A., Ono, T., Peng, S., Peters, W., Pfeil, B., Poulter, B., Raupach, M. R., Regnier, P., Rödenbeck, C., Saito, S., Salisbury, J. E., Schuster, U., Schwinger, J., Séférian, R., Segschneider, J., Steinhoff, T., Stocker, B. D., Sutton, A. J., Takahashi, T., Tilbrook, B., van der Werf, G. R., Viovy, N., Wang, Y.-P., Wanninkhof, R., Wiltshire, A., and Zeng, N.: Global carbon budget 2014, *Earth Syst. Sci. Data*, 7, 47–85, doi:10.5194/essd-7-47-2015, 2015.
- Levitus, S., Antonov, J., and Boyer, T.: Warming of the world ocean, 1955–2003, *Geophys. Res. Lett.*, 32, L02604, doi:10.1029/2004gl021592, 2005.
- Locarnini, R. A., Mishonov, A. V., Antonov, J. I., Boyer, T. P., Garcia, H. E., Baranova, O. K., Zweng, M. M., Paver, C. R., Reagan, J. R., Johnson, D. R., Hamilton, M., and Seidov, D.: World Ocean Atlas 2013, Volume 1: Temperature, edited by: S. Levitus, E., and A. Mishonov, T. E., NOAA Atlas NESDIS 73, 40 pp. 2013.
- Lyman, J. M., Good, S. A., Gouretski, V. V., Ishii, M., Johnson, G. C., Palmer, M. D., Smith, D. M., and Willis, J. K.: Robust warming of the global upper ocean, *Nature*, 465, 334–337, doi:10.1038/nature09043, 2010.
- Mathis, J. T. and Questel, J. M.: Assessing seasonal changes in carbonate parameters across small spatial gradients in the Northeastern Chukchi Sea, *Cont. Shelf Res.*, 67, 42–51, doi:10.1016/j.csr.2013.04.041, 2013.
- McNeil, B. I. and Matear, R. J.: Southern Ocean acidification: A tipping point at 450-ppm atmospheric CO₂, *P. Natl. Acad. Sci. USA*, 105, 18860–18864, doi:10.1073/pnas.0806318105, 2008.
- McNeil, B. I. and Matear, R. J.: The non-steady state oceanic CO₂ signal: its importance, magnitude and a novel way to detect it, *Biogeosciences*, 10, 2219–2228, doi:10.5194/bg-10-2219-2013, 2013.
- McNeil, B. I., Tagliabue, A., and Sweeney, C.: A multi-decadal delay in the onset of corrosive “acidified” waters in the Ross Sea of Antarctica due to strong air-sea CO₂ disequilibrium, *Geophys. Res. Lett.*, 37, L19607, doi:10.1029/2010gl044597, 2010.
- Mehrbach, C., Culbertson, C. H., Hawley, J. E., and Pytkowicz, R. M.: Measurement of the Apparent Dissociation Constants of Carbonic Acid in Seawater at Atmospheric Pressure, *Limnol. Oceanogr.*, 18, 897–907, 1973.
- Meinshausen, M., Smith, S. J., Calvin, K., Daniel, J. S., Kainuma, M. L. T., Lamarque, J. F., Matsumoto, K., Montzka, S. A., Raper, S. C. B., Riahi, K., Thomson, A., Velders, G. J. M., and Vuuren, D. P. P.: The RCP greenhouse gas concentrations and their extensions from 1765 to 2300, *Climatic Change*, 109, 213–241, doi:10.1007/s10584-011-0156-z, 2011.
- Monteiro, P., Schuster, U., Hood, M., Lenton, A., Metzl, N., Olsen, A., Rogers, K., Sabine, C., Takahashi, T., Tilbrook, B., Yoder, J., Wanninkhof, R., and Watson, A. J.: A Global Sea Surface Carbon Observing System: Assessment of Changing Sea Surface CO₂ and Air-Sea CO₂ Fluxes, *Proceedings of OceanObs’09: Sustained Ocean Observations and Information for Society (Vol. 2)*, Venice, Italy, 21–25 September 2009, 2010.
- Mucci, A.: The solubility of calcite and aragonite in seawater at various salinities, temperatures, and one atmosphere total pressure, *Am. J. Sci.*, 283, 780–799, doi:10.2475/ajs.283.7.780, 1983.
- Newton, J. A., Feely, R. A., Jewett, E. B., Williamson, P., and Mathis, J.: Global Ocean Acidification Observing Network: Requirements and Governance Plan, available at: http://goa-on.org/docs/GOA-ON_plan_print.pdf (last access: August 2015), First Edn., 60 pp., 2014.
- Orr, J. C., Fabry, V. J., Aumont, O., Bopp, L., Doney, S. C., Feely, R. A., Gnanadesikan, A., Gruber, N., Ishida, A., Joos, F., Key, R. M., Lindsay, K., Maier-Reimer, E., Matear, R., Monfray, P., Mouchet, A., Najjar, R. G., Plattner, G.-K., Rodgers, K. B., Sabine, C. L., Sarmiento, J. L., Schlitzer, R., Slater, R. D., Totterdell, I. J., Weirig, M.-F., Yamanaka, Y., and Yool, A.: Anthropogenic ocean acidification over the twenty-first century and its impact on calcifying organisms, *Nature*, 437, 681–686, doi:10.1038/nature04095, 2005.
- Palmer, J. R. and Totterdell, I. J.: Production and export in a global ocean ecosystem model, *Deep-Sea Res. Pt. I*, 48, 1169–1198, doi:10.1016/S0967-0637(00)00080-7, 2001.
- Pilcher, D. J., Brody, S. R., Johnson, L., and Bronselaer, B.: Assessing the abilities of CMIP5 models to represent the seasonal cycle of surface ocean pCO₂, *J. Geophys. Res.-Oceans*, 120, 4625–4637, doi:10.1002/2015JC010759, 2015.
- Popova, E. E., Yool, A., Aksenov, Y., Coward, A. C., and Anderson, T. R.: Regional variability of acidification in the Arctic: a sea of contrasts, *Biogeosciences*, 11, 293–308, doi:10.5194/bg-11-293-2014, 2014.
- Ricke, K. L., Orr, J. C., Schneider, K., and Caldeira, K.: Risks to coral reefs from ocean carbonate chemistry changes in recent earth system model projections, *Environ. Res. Lett.*, 8, 034003, doi:10.1088/1748-9326/8/3/034003, 2013.
- Riley, J. P. and Tongudai, M.: The major cation/chlorinity ratios in sea water, *Chem. Geol.*, 2, 263–269, doi:10.1016/0009-2541(67)90026-5, 1967.
- Sarma, V. V. S. S., Lenton, A., Law, R. M., Metzl, N., Patra, P. K., Doney, S., Lima, I. D., Dlugokencky, E., Ramonet, M., and Valsala, V.: Sea-air CO₂ fluxes in the Indian Ocean between 1990

- and 2009, *Biogeosciences*, 10, 7035–7052, doi:10.5194/bg-10-7035-2013, 2013.
- Sarmiento, J. L. and Gruber, N.: Sinks for Anthropogenic Carbon, *Phys. Today*, 55, 30–36, doi:10.1063/1.1510279, 2002.
- Sarmiento, J. L. and Gruber, N.: *Ocean biogeochemical dynamics*, Princeton University Press, Princeton, New Jersey, 526 pp., 2006.
- Sasse, T. P., McNeil, B. I., and Abramowitz, G.: A new constraint on global air-sea CO₂ fluxes using bottle carbon data, *Geophys. Res. Lett.*, 40, 1594–1599, doi:10.1002/grl.50342, 2013a.
- Sasse, T. P., McNeil, B. I., and Abramowitz, G.: A novel method for diagnosing seasonal to inter-annual surface ocean carbon dynamics from bottle data using neural networks, *Biogeosciences*, 10, 4319–4340, doi:10.5194/bg-10-4319-2013, 2013b.
- Schlitzer, R.: *Ocean Data View*, <http://odv.awi.de> (last access: February 2014), 2013.
- Schuster, U., Watson, A. J., Bates, N. R., Corbiere, A., Gonzalez-Davila, M., Metzl, N., Pierrot, D., and Santana-Casiano, M.: Trends in North Atlantic sea-surface *f*CO₂ from 1990 to 2006, *Deep-Sea Res. Pt. II*, 56, 620–629, doi:10.1016/j.dsr2.2008.12.011, 2009.
- Secretariat of the Convention on Biological Diversity: *An Updated Synthesis of the Impacts of Ocean Acidification on Marine Biodiversity*, edited by: Hennige, S., Roberts, J. M., and Williamson, P., Technical Series no. 75, Montreal, 99 pp. 2014.
- Séférian, R., Bopp, L., Gehlen, M., Orr, J., Ethé, C., Cadule, P., Aumont, O., Salas y Méliá, D., Voltaire, A., and Madec, G.: Skill assessment of three earth system models with common marine biogeochemistry, *Clim. Dynam.*, 40, 2549–2573, doi:10.1007/s00382-012-1362-8, 2013.
- Shaw, E. C., Munday, P. L., and McNeil, B. I.: The role of CO₂ variability and exposure time for biological impacts of ocean acidification, *Geophys. Res. Lett.*, 40, 4685–4688, doi:10.1002/grl.50883, 2013.
- Steinacher, M., Joos, F., Frölicher, T. L., Plattner, G.-K., and Doney, S. C.: Imminent ocean acidification in the Arctic projected with the NCAR global coupled carbon cycle-climate model, *Biogeosciences*, 6, 515–533, doi:10.5194/bg-6-515-2009, 2009.
- Takahashi, T., Sutherland, S. C., Wanninkhof, R., Sweeney, C., Feely, R. A., Chipman, D. W., Hales, B., Friederich, G., Chavez, F., Sabine, C. L., Watson, A., Bakker, D. C. E., Schuster, U., Metzl, N., Yoshikawa-Inoue, H., Ishii, M., Midorikawa, T., Nojiri, Y., Körtzinger, A., Steinhoff, T., Hoppema, M., Olafsson, J., Arnarson, T. S., Tilbrook, B., Johannessen, T., Olsen, A., Bellerby, R. G. J., Wong, C. S., Delille, B., Bates, N. R., and de Baar, H. J. W.: Climatological mean and decadal change in surface ocean *p*CO₂, and net sea-air CO₂ flux over the global oceans, *Deep-Sea Res. Pt. II*, 56, 554–577, doi:10.1016/j.dsr2.2008.12.009, 2009.
- Takahashi, T., Sutherland, S. C., Chipman, D. W., Goddard, J. G., Ho, C., Newberger, T., Sweeney, C., and Munro, D. R.: Climatological distributions of pH, *p*CO₂, total CO₂, alkalinity, and CaCO₃ saturation in the global surface ocean, and temporal changes at selected locations, *Mar. Chem.*, 164, 95–125, doi:10.1016/j.marchem.2014.06.004, 2014.
- Tjiputra, J. F., Olsen, A., Bopp, L., Lenton, A., Pfeil, B., Roy, T., Segsneider, J., Totterdell, I., and Heinze, C.: Long-term surface *p*CO₂ trends from observations and models, *Tellus B*, 66, doi:10.3402/tellusb.v66.23083, 2014.
- Tupper, M., Tan, M. K., Tan, S. L., Radius, M. J., and Abdullah, S.: ReefBase: a global information system on coral reefs, <http://www.reefbase.org> (last access: October 2013), 2011.
- Zahariev, K., Christian, J. R., and Denman, K. L.: Preindustrial, historical, and fertilization simulations using a global ocean carbon model with new parameterizations of iron limitation, calcification, and N₂ fixation, *Prog. Oceanogr.*, 77, 56–82, doi:10.1016/j.pocean.2008.01.007, 2008.
- Zweng, M. M., Reagan, J. R., Antonov, J. I., Locarnini, R. A., Mishonov, A. V., Boyer, T. P., Garcia, H. E., Baranova, O. K., Johnson, D. R., Seidov, D., and Biddle, M. M.: *World Ocean Atlas 2013, Volume 2: Salinity*, edited by: Levitus, S. and Mishonov, A., NOAA Atlas NESDIS 74, 39 pp., 2013.